Raman and infrared spectroscopic studies of the $Li_3Na_3In_2F_{12}$ fluoride garnet

2002 J. Phys.: Condens. Matter 14 271

(http://iopscience.iop.org/0953-8984/14/2/313)

INSTITUTE OF PHYSICS PUBLISHING JOURNAL OF PHYSICS: CONDENSED MATTER

J. Phys.: Condens. Matter **14** (2002) 271–280 PII: S0953-8984(02)26954-4

Raman and infrared spectroscopic studies of the $Li_3Na_3In_2F_{12}$ fluoride garnet

M A C Machado[1], C W A Paschoal[1], J Mendes Filho[1], A P Ayala[1,4], R L Moreira[2] and J-Y Gesland[3]

[1] Departamento de Física, Universidade Federal do Ceará, CP 6030, 60451-970 Fortaleza, Ceará, Brazil
[2] Departamento de Física, ICEx, Universidade Federal de Minas Gerais, CP 702, 30123-970 Belo Horizonte, Minas Gerais, Brazil
[3] Université du Maine-Cristallogenèse, URA 807, 72017 Le Mans Cedex, France

E-mail: ayala@fisica.ufc.br

Received 12 July 2001, in final form 12 November 2001
Published 13 December 2001
Online at stacks.iop.org/JPhysCM/14/271

Abstract

Single crystals of the $Li_3Na_3In_2F_{12}$ fluoride garnet have been studied by Fourier-transform infrared spectroscopy and Raman scattering. Polarized Raman spectra were recorded at low temperatures showing that the room-temperature phase is stable down to 7 K. Selected scattering geometries allow us to identify the Raman-active phonons based on the factor group analysis. The infrared reflectance spectrum was measured at room temperature and analysed on the basis of the four-parameter semi-quantum model.

1. Introduction

The optical properties of Cr^{3+}-doped fluoride crystals have attracted much attention over the past 20 years. In fluoride crystals the crystalline field is weaker than those in oxide hosts and, accordingly, the $^4T_2 \rightarrow {}^4A_2$ broad-band emission generally predominates. Attractive features of these materials include long upper-state lifetimes, which permit their use as efficient amplifying media, and absorption bands in the red region, which allow direct diode pumping.

$Li_3Na_3M_2F_{12}$ (M = Al, Fe, Ga and In) fluoride garnets have been largely studied because trivalent ions, generally Cr^{3+}, can be placed in six-coordinated sites [1–5]. Since the lower the Cr–F distance the higher the crystalline field, by using large M ions it is possible to place Cr^{3+} in sites with weak crystalline field. Thus, the fluoride garnet containing In^{3+}, whose ionic radius (r) is 0.93 Å, shows the largest size difference from Cr^{3+} ($r = 0.75$ Å) when compared with other metals. This size difference suggests that in $Li_3Na_3In_2F_{12}$ crystals, Cr^{3+} ions are submitted to a weak crystalline field; thus a wide emission band should be expected.

[4] Corresponding author.

Furthermore, the garnet structure provides a large number of phonons, which benefit the broadening of the chromium emission band.

The optical properties of the $Li_3Na_3In_2F_{12}$ were first reported by de Viry *et al* [6, 7]. The emission spectrum showed a broad emission band between 700 and 1000 nm with a long and purely radiative lifetime, which increases at low temperatures. These authors also suggested that the temperature dependence of the radiative lifetime should be associated with a strong phonon coupling dependence on temperature [6]. Moreover, the radiative lifetime remains constant at moderate hydrostatic pressures, but it increases quickly after the transition from low to high crystalline field, which is characterized by the crossing of the $^2E_2$ and $^4T_2$ energy levels [8]. Afterwards, de Viry *et al* verified that Cr^{3+} ions occupy sites with a slightly distorted octahedral crystalline field [9] and extended the $Li_3Na_3In_2F_{12}$ excitation spectrum to the region of the ultraviolet and vacuum ultraviolet energies, by using a synchrotron radiation light source [10]. As pointed out by Aramburu *et al* [11], some bands of the extended excitation spectrum can be associated with charge-transfer bands, which originate in transition metal complexes with O_h symmetry and are much more intense than those due to crystal-field transitions. As charge-transfer bands in halide host lattices usually appear outside the optical region, there are few experimental studies reported on this field. In this way, the results of de Viry *et al* motivated several theoretical studies dealing with the charge-transfer process in $Li_3Na_3In_2F_{12}$ crystals [11–13].

In spite of the fundamental role of phonons in the optical spectra, a detailed study of the vibrational spectra of fluoride garnets is still lacking. Hence, in this paper we report on our investigations of infrared reflectance and polarized Raman scattering in $Li_3Na_3In_2F_{12}$ single crystals. In particular, low-temperature Raman spectra have been obtained from room temperature down to 7 K, showing the absence of any structural phase transition in this temperature range.

2. Experiment

$Li_3Na_3In_2F_{12}$ single crystals of various sizes have been pulled from stoichiometric melts using the Czochralski technique. The crystals were oriented and cut with faces perpendicular to [001], [110] and [$\bar{1}$10] directions, denoted respectively by z, x' and y'.

Micro-Raman measurements were performed using a T64000 Jobin–Yvon spectrometer equipped with an Olympus microscope and a LN_2-cooled CCD to detect the scattered light. The spectra were excited with an argon ion laser ($\lambda = 514.5$ nm). The spectrometer slits were set to give a spectral resolution better than 2 cm^{-1}. All measurements were performed using a long-working-distance plano achromatic objective (20x/0.35, 20.5 mm). Scattering geometries for the spectra listed in the text and figures follow the usual Porto notation, $a(bc)d$ [14]. Low-temperature measurements were made using an Air Products closed-cycle refrigerator coupled with a Lakeshore controller, which provides controlled temperatures ranging from 7 to 300 K.

Reflection infrared spectra were recorded with a BOMEM DA8 Fourier transform spectrometer, in the wavenumber range 10–4000 cm^{-1}. The spectral resolution was typically 4 cm^{-1}. For the mid-infrared region (above 500 cm^{-1}), the better choice of accessories was a Globar source, a KBr beamsplitter and a LN_2-cooled HgCdTe detector. The far-infrared region was measured using a Globar or a Mercurium arc lamp (below 200 cm^{-1}), a 6 μm coated-mylar Hypersplitter^{TM} and a LHe-cooled Si bolometer.

3. Crystalline structure and group theory analysis

$Li_3Na_3In_2F_{12}$ crystals are isostructural to the quaternary fluoride garnet family (cryolithionite structure [15]), which, according to Massa *et al* [16], belongs to the cubic $Ia\bar{3}d$ (O_h^{10}) space group. The lattice parameter is 12.693 Å with eight formulae per unit cell. In this structure, lithium, sodium, indium and fluorine ions occupy 24d, 24c, 16a and 96h sites, respectively.

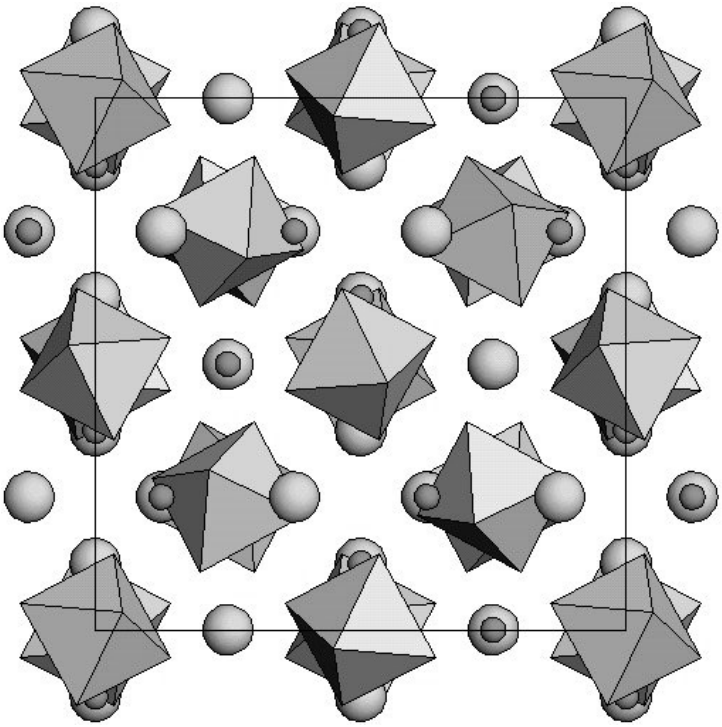

Figure 1. Crystalline structure of the $Li_3Na_3In_2F_{12}$ fluoride garnet. Octahedra represent InF_6^{3-} anions, while smaller and larger spheres correspond to lithium and sodium cations, respectively.

Moreover, indium has an octahedral coordination as can be observed in figure 1. InF_6 octahedra are slightly elongated along the $\bar{3}$ axis, presenting a trigonal distortion. These octahedra do not share the fluorine ions and are arranged in planes parallel to the {110} family.

Based on the reported crystalline structure of $Li_3Na_3In_2F_{12}$ and using the method of site group analysis proposed by Rousseau *et al* [17], the distribution of the degrees of freedom in irreducible representations of the O_h factor group was calculated and is presented in table 1. For this factor group, acoustic and infrared modes belong to the F_{1u} irreducible representation, while A_{1g}, E_g and F_{2g} modes are Raman active. The polarizability tensors of the Raman-active modes are as follows:

$$A_{1g}: \begin{pmatrix} a & \cdot & \cdot \\ \cdot & a & \cdot \\ \cdot & \cdot & a \end{pmatrix}$$

$$E_g: \begin{pmatrix} b & \cdot & \cdot \\ \cdot & -b & \cdot \\ \cdot & \cdot & -2b \end{pmatrix} \qquad \begin{pmatrix} -\sqrt{3}b & \cdot & \cdot \\ \cdot & -\sqrt{3}b & \cdot \\ \cdot & \cdot & \cdot \end{pmatrix}$$

$$F_{2g}: \begin{pmatrix} \cdot & \cdot & \cdot \\ \cdot & \cdot & d \\ \cdot & d & \cdot \end{pmatrix} \qquad \begin{pmatrix} \cdot & \cdot & d \\ \cdot & \cdot & \cdot \\ d & \cdot & \cdot \end{pmatrix} \qquad \begin{pmatrix} \cdot & d & \cdot \\ d & \cdot & \cdot \\ \cdot & \cdot & \cdot \end{pmatrix}.$$

The relative intensities of the modes calculated from the Raman polarizability tensors in the different backscattering geometries are summarized in table 2. Notice that when the incident and the outgoing beams are both polarized parallel to the same crystallographic axis a mixture of phonons belonging to A_{1g} and E_g irreducible representations is observed, while

Table 1. Factor group analysis of the $Li_2Na_2In_3F_{12}$ structure.

Atom	Site	Irreducible representations
Li	S_4	$A_{1u} \oplus A_{2g} \oplus E_g \oplus E_u \oplus 2F_{1g} \oplus 3F_{1u} \oplus 3F_{2g} \oplus 2F_{2u}$
Na	D_2'	$A_{2g} \oplus A_{2u} \oplus E_g \oplus E_u \oplus 3F_{1g} \oplus 3F_{1u} \oplus 2F_{2g} \oplus 2F_{2u}$
In	S_6	$A_{1u} \oplus A_{2u} \oplus 2E_u \oplus 3F_{1u} \oplus 3F_{2u}$
F	C_1	$3A_{1g} \oplus 3A_{1u} \oplus 3A_{2g} \oplus 3A_{2u} \oplus 6E_g \oplus 6E_u \oplus$ $\oplus 9F_{1g} \oplus 9F_{1u} \oplus 9F_{2g} \oplus 9F_{2u}$
Total		$\Gamma = 3A_{1g} \oplus 5A_{1u} \oplus 5A_{2g} \oplus 5A_{2u} \oplus 8E_g \oplus 10E_u \oplus$ $\oplus 14F_{1g} \oplus 18F_{1u} \oplus 14F_{2g} \oplus 16F_{2u}$
Acoustic		$\Gamma_{ac} = F_{1u}$
Raman		$\Gamma_R = 3A_{1g} \oplus 8E_g \oplus 14F_{2g}$
Infrared		$\Gamma_{IR} = 17F_{1u}$

Table 2. Intensity of the Raman-active modes in the different backscattering configurations.

Configuration	A_{1g}	E_g	F_{2g}
$z(xx)\bar{z}$	a^2	$4b^2$	0
$z(xy)\bar{z}$	0	0	d^2
$z(x'y')\bar{z}$	0	b^2	0
$z(x'x')\bar{z}$	a^2	$3b^2$	d^2

Table 3. Phonon wavenumber (cm^{-1}) of the bands observed in the Raman spectra at 7 and 300 K, in the $z(xx)\bar{z}$ scattering geometry.

7 K	90	158	215	260	302	371	385	451	471	489	520
300 K	90	158	215	260	303	371	386	452			519

if they are polarized parallel to different crystallographic axes the F_{2g} modes are detected. In order to discriminate between A_{1g} and E_g modes light polarized according to x' and y' can be used. In fact, the crossed polarization geometry $z(x'y')\bar{z}$ allows the observation of E_g modes only, while in the parallel $z(x'x')\bar{z}$ geometry all Raman-active modes should be detected. In this way, polarized Raman measurements in the first three scattering geometries listed in table 2 suffice to distinguish between the three allowed symmetries of the Raman-active modes.

4. Results and discussion

4.1. Raman scattering

Raman spectra were recorded between 7 and 300 K in order to study the temperature behaviour of the $Li_3Na_3In_2F_{12}$ phonon spectrum. Figure 2 shows some selected spectra obtained in the $z(xx)\bar{z}$ scattering geometry. As expected in fluoride crystals, all vibrational modes are located below 700 cm^{-1}. Furthermore, figure 2 shows no temperature dependence of the Raman frequencies, within the experimental error of 2 cm^{-1} (see table 3). This behaviour, as well as the absence of any evidence of a structural phase transition, is confirmed in the other scattering geometries.

Since no phase transition was observed and the phonon frequencies do not depend on the temperature, we use the spectra recorded at 7 K (which present the most intense and narrowest bands) to classify the vibrational modes according to the irreducible representations of the O_h point group. Figure 3 shows the Raman spectra of $Li_3Na_3In_2F_{12}$ crystals at 7 K in the $z(xx)\bar{z}$,

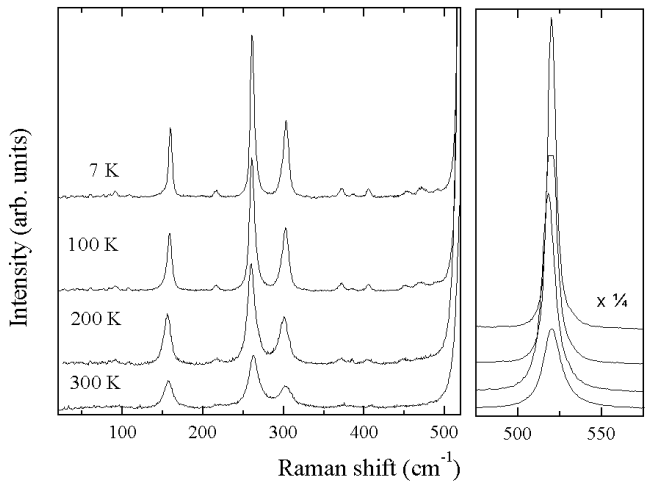

Figure 2. Selected Raman spectra of $Li_3Na_3In_2F_{12}$ crystal at low temperatures, for the $z(xx)\bar{z}$ scattering geometry.

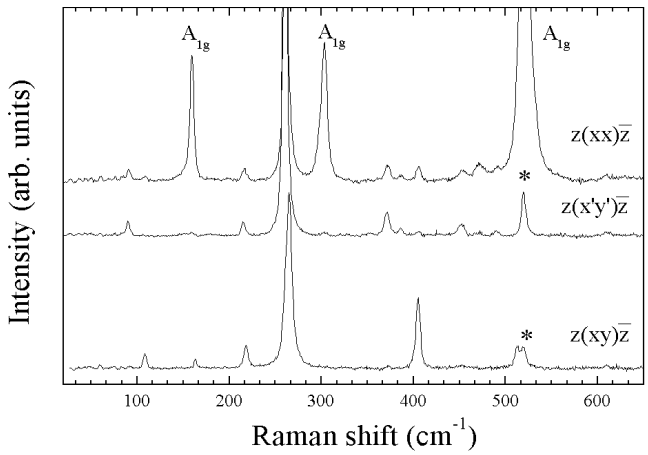

Figure 3. Raman spectra at 7 K recorded in the $z(xx)\bar{z}$, $z(x'y')\bar{z}$ and $z(xy)\bar{z}$ scattering geometries. The asterisk denotes the peak leakage of the strong 520 cm^{-1} A_{1g} mode.

$z(x'y')\bar{z}$ and $z(xy)\bar{z}$ scattering geometries. Based on the factor group analysis, Raman-active phonons are distributed in the following way:

$$z(xx)\bar{z} \;:\; 3A_{1g} \oplus 8E_g$$
$$z(x'y')\bar{z} \;:\; 8E_g$$
$$z(xy)\bar{z} \;:\; 14F_{2g}.$$

By comparing the results obtained in the $z(xx)\bar{z}$ and $z(x'y')\bar{z}$ scattering geometries, the A_{1g} and E_g modes can be easily identified. Thus, the bands located at 159, 302 and 520 cm^{-1} are observed in the $z(xx)\bar{z}$ spectrum, but only the last band is weakly present in the $z(x'y')\bar{z}$ spectrum. Thus, we conclude that these bands belong to the A_{1g} irreducible representation and that the strongest band in the $z(xx)\bar{z}$ spectrum is observed as a polarization leak in the $z(x'y')\bar{z}$ geometry. The other eight bands measured in the $z(x'y')\bar{z}$ geometry correspond to

Table 4. Phonon wavenumbers of the $Li_3Na_3In_2F_{12}$ Raman-active modes measured at 7 K.

A_{1g} (cm^{-1})	E_g (cm^{-1})	F_{2g} (cm^{-1})
158	90	59
302	215	108
520	260	163
	371	217
	385	264
	451	372
	471	404
	489	452
		512

phonons belonging to the E_g irreducible representation. The most intense A_{1g} band leaks again in the $z(xy)\bar{z}$ spectrum, where only the F_{2g} phonons are predicted by the factor group analysis. The wavenumber of the measured phonons as well as their assignment to the irreducible representation of the O_h point group are presented in the table 4. As a consequence of our analysis all A_{1g} and E_g vibrational modes were identified, while nine of the 14 predicted F_{2g} modes were observed.

For a regular octahedral InF_6^{3-} anion with O_h symmetry, three stretching modes ν_1 (A_{1g}), ν_2 (E_g) and ν_3 (F_{1u}) and three bending modes ν_4 (F_{1u}), ν_5 (F_{2g}) and ν_6 (F_{2u}) are allowed, where ν_1, ν_2 and ν_5 are Raman-active modes, ν_3 and ν_4 are infrared-active modes and ν_6 is a silent mode. In general, the order of the stretching frequencies is $\nu_1 > \nu_3 > \nu_2$ or $\nu_3 > \nu_1 > \nu_2$, while the order of bending frequencies is $\nu_4 > \nu_5 > \nu_6$ [18, 19]. Since in the $Li_3Na_3In_2F_{12}$ structure the InF_6^{3-} anions are slightly distorted with an S_6 symmetry, the influence of the lowering of the octahedral symmetry in the vibrational spectra should be analysed by using the corresponding correlation diagram, which is shown in table 5.

From table 5, we observe that the A_{1g} modes correspond to either librational or internal vibrations of the InF_6^{3-} octahedra. Thus, it is straightforward to assign the phonons at 158, 302 and 520 cm^{-1} to the librational, the ν_5 and the ν_1 modes, respectively, in agreement with previously reported results [20, 21]. Six E_g modes originate in octahedral vibrations, which are distributed as two librations, two ν_2 and two ν_5 modes, the remaining modes being due to lithium and sodium translations, as can be observed in table 1. Nevertheless, as lithium and sodium are light atoms, their corresponding vibrational modes can appear in the intermediate-frequency range. Thus, as an example, we can cite the results obtained by Salaün *et al* in $LiYF_4$, where the one-phonon density of state of lithium cations is close to zero below 200 cm^{-1} [22]. Furthermore, since fluorine anion is much less massive than the indium cation, the F_{2g} bending frequencies are expected below the asymmetric E_g stretching mode, which in turn should be below the symmetric A_{1g} stretching mode. Following these arguments, the higher-frequency E_g modes should be classified as two ν_2 modes, but the assignment of the ν_5 is not clear. Based on the classification of the A_{1g} modes, we presume that the modes around 300 cm^{-1} are the ν_5 vibrations, but it is hard to obtain a correct assignment without the help of lattice dynamic calculations. A similar situation holds for the F_{2g} modes, which are composed by three librations, two ν_5, two ν_2 and two ν_1 modes of the InF_6^{3-} octahedra, together with five translations of the lithium and sodium cations. Moreover, only nine of the 14 F_{2g} modes were observed. However, based on previous results [20,21], the modes around 300 and 512 cm^{-1} can be assigned to ν_5 and ν_1 vibrations of the InF_6^{3-} octahedra, respectively. ν_2 internal vibrations are expected around 490 cm^{-1}, but they are usually weak and were not observed in the present work.

Table 5. Correlation diagram of the InF_6^{-3} anion in the S_6 site of the O_h^{10} space group. In the third column, only the Raman- and infrared-active irreducible representations are shown.

InF_6^{-2} symmetry	Site symmetry	Crystal symmetry	Vibrational modes
O_h	S_6	O_h	
$A_{1g}(\nu_1)$			
$E_g(\nu_2)$	A_g	A_{1g}	R, ν_1, ν_5
$F_{1g}(R)$		E_g	$2R, 2\nu_2, 2\nu_5$
	E_g	F_{2g}	$3R, 2\nu_1, 2\nu_2, 2\nu_5$
$F_{2g}(\nu_5)$			
	A_u		
$F_{2u}(\nu_6)$		F_{1u}	$3T, 3\nu_3, 3\nu_4, 3\nu_6$
	E_u		
$F_{1u}(T, \nu_3, \nu_4)$			

4.2. Infrared spectroscopy

The infrared dielectric function was determined from the reflectance spectrum by using the four-parameter semiquantum model [23]. According to this model, the complex dielectric constant is expressed in terms of the infrared-active modes as follows:

$$\varepsilon(\omega) = \varepsilon_\infty \prod_j \frac{\omega_{j\mathrm{LO}}^2 - \omega^2 + \mathrm{i}\omega\gamma_{j\mathrm{LO}}}{\omega_{j\mathrm{TO}}^2 - \omega^2 + \mathrm{i}\omega\gamma_{j\mathrm{TO}}} \tag{1}$$

where $\omega_{j\mathrm{TO}}$ and $\omega_{j\mathrm{LO}}$ correspond to the resonance frequencies of the jth transverse and longitudinal modes, respectively, and $\gamma_{j\mathrm{TO}}$ and $\gamma_{j\mathrm{LO}}$ are the corresponding damping factors. ε_∞ is the dielectric constant due to electronic polarizations. For normal incidence, the infrared reflectivity $\boldsymbol{R}$ and the dielectric function are related by

$$\boldsymbol{R} = \left| \frac{\sqrt{\varepsilon} - 1}{\sqrt{\varepsilon} + 1} \right|^2 . \tag{2}$$

The experimental and calculated infrared reflectivities of $Li_3Na_3In_2F_{12}$ are presented in figure 4, showing a relatively good agreement between the measured and calculated curves [24]. Table 6 lists the frequencies and dampings of transversal and longitudinal optical modes of the best fit to the reflectivity curve. The oscillator strength $\Delta\varepsilon_{j\mathrm{TO}}$ of the jth transversal mode can

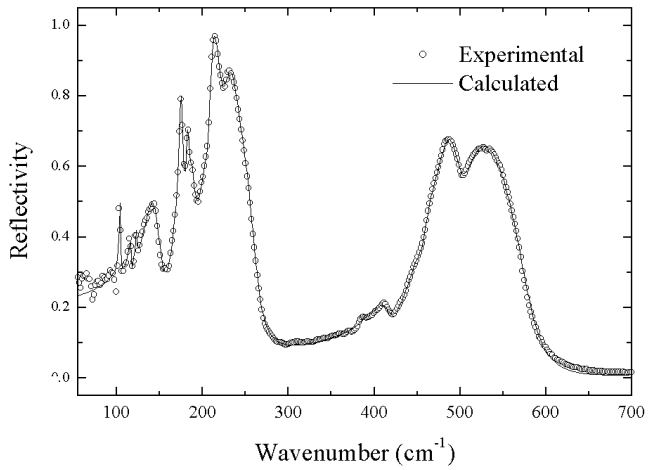

Figure 4. Infrared reflectivity of $Li_3Na_3In_2F_{12}$ single crystals.

Table 6. Dispersion parameters for the best fit to the reflectivity data of $Li_3Na_3In_2F_{12}$ crystals at 300 K.

ω_{TO} (cm^{-1})	γ_{TO} (cm^{-1})	ω_{LO} (cm^{-1})	γ_{LO} (cm^{-1})	$\Delta\varepsilon_{TO}$
103.8	0.9	104.0	2.6	0.054
116.5	2.2	117.0	2.5	0.121
122.8	1.9	122.9	2.7	0.026
141.5	12.1	154.5	19.8	2.041
174.5	1.0	179.2	4.9	1.030
181.4	2.8	186.7	2.5	0.428
186.8	2.2	195.4	16.3	0.018
199.1	11.2	204.6	51.1	0.129
209.2	4.4	220.3	24.8	0.187
227.1	17.0	245.9	47.7	0.163
252.6	29.4	260.7	25.9	0.035
386.7	4.7	386.8	5.2	0.003
414.0	20.5	417.1	18.7	0.088
448.6	18.8	451.4	19.6	0.127
462.8	17.4	466.7	31.0	0.198
476.2	27.8	498.4	27.1	0.435
505.0	33.8	579.8	41.7	0.124
$\varepsilon_\infty = 1.902$		$\varepsilon_0 = 7.109$		

be directly deduced from the LO–TO splitting through the relation

$$\Delta\varepsilon_{j\mathrm{TO}} = \frac{\varepsilon_\infty}{\omega_{j\mathrm{TO}}^2} \times \frac{\prod_k (\omega_{k\mathrm{LO}}^2 - \omega_{k\mathrm{TO}}^2)}{\prod_{k\neq j} (\omega_{k\mathrm{TO}}^2 - \omega_{j\mathrm{TO}}^2)}. \tag{3}$$

Furthermore, the static dielectric constant can be obtained by adding the strength of all oscillators, that is

$$\varepsilon_0 = \varepsilon_\infty + \sum_k \Delta\varepsilon_{j\mathrm{TO}}. \tag{4}$$

Transmission infrared spectra of pellets of various fluoride garnets have been previously studied by Langley and Sturgeon [25]. Since these authors used the transmittance technique,

Table 7. Assignment of the vibronic bands (in cm^{-1}) to the $Li_3Na_3In_2F_{12}$ phonon spectra (in cm^{-1}).

Emission spectra[a]	Phonon spectra	Assignment
60	59 (R)	Lattice
220	220 (IR)	ν_6
300	300 (R)	ν_5
470	471 (R)	ν_2
530	512 (R)	ν_1
600	579 (IR)	ν_3
720		$\nu_1 + \nu_6$

[a] From [6] and [8].

they were not able to identify either the TO–LO splitting or the corresponding damping factors. However, their results clearly show a lattice parameter dependence of the MF_6 infrared modes. Transmittance and reflectance results can be compared by noticing that the absorption coefficient is proportional to the imaginary part of the refractive index, which peaks at approximately ω_{TO}. Moreover, the $Li_3Na_3In_2F_{12}$ lattice parameter has a larger unit cell than the compounds reported in [25]. In this way, by comparing the first column of our table 6 with the Langley and Sturgeon results [25], we observe that the main behaviour of the infrared-active modes is retained (see figure 1 of [25]) when the lattice parameter increases; i.e., the phonon frequencies of the modes below 300 cm^{-1} or above 450 cm^{-1} decrease, while the frequencies of those between 300 and 450 cm^{-1} remain approximately constant. This allows us to conclude that the modes of the MF_6^{3-} octahedra are those located below 300 cm^{-1} or above 450 cm^{-1}.

Since in the O_h point group only the triply degenerate F_{1u} irreducible representations are infrared active, our factor group analysis predicts that 17 vibrational modes should be measured by infrared spectroscopy. As can be observed in table 6, all the predicted vibrational modes could be identified. Following the factor group analysis (table 1) and the InF_6^{3-} correlation diagram (table 5) we notice that the infrared active modes are composed by five translations of the lithium and sodium cations, besides three translations, three ν_3, three ν_4 and three ν_6 of the InF_6^{3-} anion. Note that the ν_6 bending modes, which are silent in a perfect octahedron, become infrared active due to the slight trigonal distortion. Based on previous results, we can associate the higher-frequency bands with the ν_3 internal modes of the InF_6^{3-} octahedra, while the bands between 200 and 300 cm^{-1} should be classified as ν_4 and ν_6 modes [20, 21].

A last remark concerns the reach vibronic structure of the photoluminescence spectrum of the chromium-doped $Li_3Na_3In_2F_{12}$ crystal, measured by de Viry *et al* [6, 8]. As in Cr^{3+}-doped A_2BMX_6 elpasolites (A, B = monovalent cation; M = trivalent cation), in the $Li_3Na_3In_2F_{12}$ structure, the octahedra are well separated and the main contribution to the vibronic spectra is due to the internal modes of the InF_6 complex [18, 26, 27]. This effect is enhanced by the chromium ion because of its stronger covalency [28]. The very low thermal expansion coefficient presented by our crystal indicated that anharmonic effects, like combination modes (two-phonon processes), are less probable. Besides, due to the trigonal octahedron distortion, the CrF_6^{3-} modes should have A_{1g}, E_g, F_{2g} or F_{1u} symmetry (table 5). Since the chromium ion substitutes the indium ions in an S_6 site, only F_{1u} modes should be affected by the presence of this lighter ion in the place of the In ion (see table 1). In consequence, the vibronic wavenumbers should be close to the corresponding $Li_3Na_3In_2F_{12}$ phonon modes. Thus, by taking these features into account a new mode assignment for the vibronic spectra of [6] and [8] is proposed in table 7, which agrees very well with the results obtained in other Cr^{3+}-doped fluoride crystals [29].

5. Conclusion

Polarized Raman and infrared reflectivity spectra of $Li_3Na_3In_2F_{12}$ single crystals allowed us to determine the complete set of three A_{1g}, eight E_g, 17 F_{1u} modes and the nine most intense of the 14 predicted F_{2g} modes. Low-temperature Raman spectra showed a negligible temperature evolution of the phonon frequencies, which means a low anharmonic character of the elastic potential. The MF_6 octahedra are slightly distorted in the S_6 cubic site, leading to a particular redistribution of their vibrational and librational modes in irreducible representations of the crystal point group. These results helped us to reinterpret the vibronic emission spectra of the chromium-doped indium garnet.

Acknowledgments

This work has been partially supported by the Brazilian agencies CNPq, FUNCAP and FAPEMIG.

References

[1] de Pape R, Portier J, Gauthier G and Hagenmuller P 1967 *C. R. Acad. Sci., Paris* C **265** 1244
[2] de Pape R, Portier J, Grannec J, Gauthier G and Hagenmuller P 1969 *C. R. Acad. Sci., Paris* C **269** 1120
[3] Caird J A, Payne S A, Staver P R, Ramponi A J, Chase L L and Krupke W F 1988 *IEEE J. Quantum Electron.* **24** 1077
[4] Naka S, Takeda Y, Sone M and Suwa Y 1975 *Chem. Lett.* **7** 653
[5] Langley R H and Sturgeon G D 1979 *J. Fluorine Chem.* **14** 1
[6] de Viry D, Denis J P, Blanzat B and Grannec J 1987 *J. Solid State Chem.* **71** 109
[7] de Viry D, Pelle F, Denis J P, Blanzat B, Grannec J and Chaminade J P 1987 *J. Fluorine Chem.* **35** 244
[8] de Viry D, Denis J P, Tercier N and Blanzat B 1987 *Solid State Commun.* **63** 1183
[9] de Viry D, Pilla O, Pelle F and Blanzat B 1991 *J. Lumin.* **48–9** 561
[10] de Viry D, Casalboni M, Palummo M and Zema N 1990 *Solid State Commun.* **76** 1051
[11] Aramburu J A, Barriuso M T and Moreno M 1996 *J. Phys.: Condens. Matter* **8** 6901
[12] Aramburu J A, Barriuso M T, Moreno M and Doclo K 1997 *Mater. Sci. Forum* **239** 223
[13] Aramburu J A, Moreno M, Doclo K, Daul C and Barriuso M T 1999 *J. Chem. Phys.* **110** 1497
[14] Porto S P S and Scott J F 1967 *Phys. Rev.* **157** 716
[15] Geller S 1971 *Am. Mineral.* **56** 18
[16] Massa W, Post B and Babel D 1982 *Z. Kristallogr.* **158** 299
[17] Rousseau D L, Bauman R P and Porto S P S 1981 *J. Raman Spectrosc.* **10** 253
[18] Greenough P and Paulusz A G 1979 *J. Chem. Phys.* **70** 1967
[19] Nakamoto K 1970 *Infrared Spectra of Inorganic and Coordination Compounds* (New York: Wiley) p 151
[20] Chodos S L, Black A M and Flint C D 1976 *J. Chem. Phys.* **65** 4816
[21] Sliwczuk U, Bartram R H, Gabbe D R and McCollum B C 1991 *J. Phys. Chem. Solids* **52** 357
[22] Salaün S, Bulou A, Rousseau M, Hennion B and Gesland J Y 1997 *J. Phys.: Condens. Matter* **9** 6957
[23] Gervais F and Echegut P 1986 *Incommensurete Phases in Dielectrics* ed R Blinc and A P Levanyuk (Amsterdam: North-Holland) p 337
[24] Meneses D D, desouza@cnrs-orleans.fr 1999 *IRFit2.0 Adjustment Program* Orleans University
[25] Langley R H and Sturgeon G D 1979 *Spectrochim. Acta* A **35** 209
[26] Duclos S J, Vohra Y K and Ruoff A L 1990 *Phys. Rev.* B **41** 5372
[27] Mortier M, Wang Q, Buzaré J Y, Rousseau M and Piriou B 1997 *Phys. Rev.* B **56** 3022
[28] Mortier M, Gesland J Y, Piriou B, Buzaré J Y and Rousseau M 1994 *Opt. Mater.* **4** 115
[29] Cieślak-Golonka M, Bartecki A and Sinha S P 1980 *Coordin. Chem. Rev.* **31** 251 and references therein